GEOPHYSICS, VOL. 69, NO. 4 (JULY-AUGUST 2004); P. 938–948, 10 FIGS., 1 TABLE.
10.1190/1.1778237

Automatic determination of the magnetization–density ratio and magnetization inclination from the joint interpretation of 2D gravity and magnetic anomalies

Carlos Alberto Mendonça*

ABSTRACT

The Poisson theorem establishes a linear relationship between the gravity and magnetic potentials arising from common dense and magnetized bodies with constant magnetization–density ratio and magnetization direction. For geological formations satisfying such constraints (i.e., the Poisson conditions), this theorem provides suitable relationships between the gravity and magnetic anomalies that are useful in interpreting the related data sets. In such applications, both magnetization–density ratio (MDR) and magnetization direction can be estimated, thus helping the subsurface geological mapping from potential field data acquired on the earth's surface. However, no existing method is fully automatic, which has hampered extensive use in routine applications. Such a drawback follows the adoption of equations that, although obeying the Poisson theorem, relate particular components of the gravity and magnetic fields, thus requiring either a known magnetization direction or the implementation of iterative procedures to determine it.

To allow one-pass estimates for both MDR and magnetization direction (more precisely, its inclination projected on the plane normal to the source strike), this paper presents simple analytical solutions for these parameters by relating suitable gravity and magnetic vector fields that are derived from the gravity and magnetic data sets. Because current geophysical surveys usually provide only a single-field component, a data processing scheme is developed to determine the required components in evaluating the desired vector fields. This is done by applying suitable linear transformations on the measured components according to well-established filtering techniques in processing gravity and magnetic data. Except for distortions from noise, the proposed method automatically determines the MDR and the projected magnetization inclination for the underlying rocks everywhere the Poisson conditions are satisfied. Two-dimensional sources are assumed, but no constraint upon their depth and cross-section shape is required. Distorted estimates only appear close to the sources where at least one of the Poisson conditions is violated. In this case, the proposed technique furnishes apparent values for the rock properties. The abrupt changes of apparent values over contacts detect edges, thus facilitating the mapping of geological boundaries.

The proposed technique is used to interpret two profiles across the Appalachian fold belt from the eastern portion of the State of Georgia, and the results are compared with some of the geological information available for the area.

INTRODUCTION

Gravity and magnetic data are usually processed and interpreted separately, and fully integrated results basically are created in the mind of the interpreter. Data interpretation in such a manner requires an interpreter experienced both on topics concerning potential field theory and the geology of the study area. To simplify the joint interpretation of data, the automatic production of auxiliary interpreting products, in the form of maps or profiles, is useful to help a less experienced interpreter or when investigating regions with poorly known geology. Fortunately, a suitable theoretical background for the joint interpretation of gravity and magnetic anomalies is well established and can serve promptly in generating such products. Because of its mathematical expression, this theory commonly is referred to as the Poisson relation (Garland, 1951; Grant and West, 1965) or the Poisson theorem, as in more recent publications (Cordell and Taylor, 1971; Chandler et al., 1981). In summary, the Poisson theorem (term adopted here) establishes a linear relationship between the gravity and

Manuscript received by the Editor November 26, 2001; revised manuscript received November 4, 2003.
*Universidade de São Paulo, Instituto de Astronomia, Geofísica e Ciências Atmosféricas, Departamento de Geofísica, Rua do Matão, 1226, São Paulo 05508-900, Brazil. E-mail: mendonca@iag.usp.br.

magnetic potentials and, by extension, between the corresponding anomalies measured in practice or derived from them by applying suitable data processing. For the joint interpretation of potential field data, the Poisson theorem has been used mainly to determine the magnetization–density ratio (MDR) (Garland, 1951; Kanasewich and Argawal, 1970; Bott and Ingles, 1972; Chandler et al., 1981; Hildebrand, 1985; Chandler and Malek, 1991) and, less often, the magnetization direction of single dense and magnetic structures (Ross and Lavin, 1966; Cordell and Taylor, 1971).

The methods based on the Poisson theorem have usually provided valuable contributions to the investigations to which they are applied. Nevertheless, none of the existing methods is fully automatic, which probably has precluded their extensive use in routine applications. Such a drawback can be traced back to the adoption of mathematical expressions relating particular field components of gravity and magnetic fields which necessarily requires a known magnetization direction when real data sets are interpreted. Since the magnetization direction is commonly not available from direct measurements, an iterative procedure must be implemented to determine it, thus precluding the development of one-pass algorithms. In some applications, a known magnetization direction, usually coincident with the inducing geomagnetic field, is assumed (Hildebrand, 1985). Especially in areas with stronger remanent magnetization, little useful information is obtained when this assumption is false. Conversely, the proposed method furnishes useful MDR estimates with no prior knowledge of the magnetization direction. Moreover, in favorable conditions, the magnetization inclination can also be obtained, thus helping the interpretation process.

The main contribution from my method is the adoption of expressions relating vectors of gravity and magnetic fields instead of single components, as is usually done. My derived expressions assume 2D homogeneous sources and, under this assumption, furnish simple analytical solutions for both MDR and magnetization inclination (MI). The derived solutions allow the automatic estimation of the related physical properties by applying linear transformations and arithmetic operations upon the measured gravity and magnetic anomalies. No inverse problem formulation, as done by Bott and Ingles (1972), is required. Since 2D sources are considered, the MI estimates denote the angle of the magnetization vector projected onto the plane normal to the source strike. It occurs because, as discussed in Appendix A, when 2D homogeneous sources are considered, only this component of the rock magnetization contributes to generate a magnetic field.

The analytical solutions for both MDR and MI parameters are derived and then used to generate synthetic model profiles over simple geophysical earth models. Disturbances from noise are addressed when the processing scheme for the automatic MDR and MI estimation is presented. Finally, the proposed method is applied to the interpretation of two gravity and magnetic profiles in the eastern portion of the State of Georgia. The results from the application with real data are discussed by considering the study of Long and Dainty (1985).

THEORY

The Poisson theorem (Blakely, 1995) relates the magnetic scalar potential, $V \equiv V(x, z)$, at a station (x, z) along a profile to the gravity potential, $U \equiv U(x, z)$, at the same position by

$$V = -p\frac{\partial U}{\partial m}, \tag{1}$$

where $\mathbf{m}$ is a constant unit vector along the magnetization direction, $\partial/\partial m$ is the directional derivative operator with respect to the magnetization direction, and p is the Poisson ratio given by

$$p = \frac{\Delta M}{G\Delta\rho}. \tag{2}$$

In equation (2), G is the gravitational constant, $\Delta\rho \equiv \Delta\rho(x', z')$ is the density contrast at point (x', z') within the source, and $\Delta M \equiv \Delta M(x', z')$ is the magnetization contrast at the same position. The quantity ΔM is regarded as the contrast of the total magnetization (induced plus remanent) of the source with respect to the background medium. Since homogeneous sources are assumed, the magnetization contrast is such that $\Delta\mathbf{M} = \Delta M\mathbf{m}$, in which bold letters denote vector quantities.

Many of the existing techniques based on the Poisson theorem map the spatial distribution of the MDR, $r \equiv \Delta M/\Delta\rho$, which, in general, is a very effective way of discriminating rock types. As discussed by Grant and West (1965), the Poisson theorem requires three conditions (the so-called Poisson conditions) to be valid: (1) the sources generating the potentials U and V must be the same; (2) the magnetization direction must be uniform within the sources; and (3) the MDR must be constant within the sources. When these conditions are satisfied, the magnetic potential V can be obtained from the derivatives of the gravity potential U or, conversely, the gravity potential U can be obtained by integrating the magnetic potential V (Baranov, 1957). Corresponding expressions for the related

Table 1. Mathematical symbols.

Symbol	Meaning
U	Gravity potential
V	Magnetic potential
$\Delta\rho$	Density contrast
ΔM	Magnetization contrast
p	Poisson ratio
r	Magnetization–density ratio (MDR)
α	Apparent magnetization inclination (MI)
η	Apparent inclination of inducing field
$\mathbf{z}$	Unit vector along vertical
$\mathbf{t}$	Unit vector along inducing field
$\mathbf{m}$	Unit vector along magnetization direction
I_g, D_g	Inclination and declination of $\mathbf{t}$
i_m, d_m	Inclination and declination of $\mathbf{m}$
(L, K, N)	Direction cosines of $\mathbf{t}$
(l, k, n)	Direction cosines of $\mathbf{m}$
$\mathbf{T}_z$	Vector magnetic field from a source with vertical magnetization
$\mathbf{T}_m$	Vector magnetic field from a source with magnetization direction $\mathbf{m}$
$\lvert\mathbf{T}_m\rvert$	Euclidean norm of vector $\mathbf{T}_m$
$T_m^{x,z}$	Components x (horizontal) and z (vertical) of $\mathbf{T}_m$
T_m^t	Total field anomaly ($\mathbf{T}_m$ component along direction t)
g_z	Gravity anomaly
∇	Gradient operator
$\partial/\partial m$	Derivative along direction $\mathbf{m}$
h	Continuation height (negative upward)
F	Direct Fourier transform
K	Fourier domain wavenumber

vector fields can promptly be obtained by applying the 2D gradient operator, $\nabla \equiv \partial/\partial x \mathbf{e}_x + \partial/\partial z \mathbf{e}_z$, on both sides of equation (1). The anomalous vector magnetic field $\mathbf{T}_m$ is thus obtained as

$$\mathbf{T}_m = p\nabla\left(\frac{\partial U}{\partial m}\right). \tag{3}$$

Similarly, the magnetic field $\mathbf{T}_z$ caused by the same sources but assuming vertical magnetization (i.e., $\Delta\mathbf{M} = \Delta M \mathbf{e}_z$) is

$$\mathbf{T}_z = p\nabla g_z, \tag{4}$$

where

$$g_z = \frac{\partial U}{\partial z}, \tag{5}$$

is the expression for the gravity anomaly, with the subscript z denoting the vertical component of the related gravity field, which is the quantity most commonly measured in gravity exploration.

The magnetic field $\mathbf{T}_z$ estimated from the gravity data will only be equal to the true field in regions where (1) the Poisson conditions are satisfied and (2) the source magnetization direction is vertical. In fact, the fields $\mathbf{T}_m$ and $\mathbf{T}_z$ never occur simultaneously at the same place since the total magnetization contrast of a given homogeneous structure does not simultaneously assume the **z** and **m** directions. Besides, in most cases **m** is not vertically aligned, thus insinuating, at first, that equation (4) is useless when interpreting real data sets. However, as demonstrated in Appendix A, when considering 2D homogeneous sources, $\mathbf{T}_m$ and $\mathbf{T}_z$ are such that

$$|\mathbf{T}_m| = |\mathbf{T}_z|, \tag{6}$$

for any magnetization direction **m**. Since the symbol $|.|$ represents the Euclidean norm, equation (6) shows that the magnetic-field magnitude from 2D homogeneous sources is invariant with the magnetization direction. As such, the information on the magnetization inclination resides solely in the inclination of the related vector magnetic field. Assuming Poisson conditions are valid, equation (4) can be substituted in equation (6) to give

$$|\mathbf{T}_m| = |p\nabla g_z| \tag{7}$$

from which the absolute value of the MDR, $|r|$, can be estimated promptly:

$$|r| = G\frac{|\mathbf{T}_m|}{|\nabla g_z|}. \tag{8}$$

As also shown in Appendix A, the angle between vectors $\mathbf{T}_m$ and $\nabla\mathbf{g}_z$ depends on the apparent MI, α, which then can be determined by

$$\alpha = \operatorname{asin}\left(\frac{\mathbf{T}_m \cdot \nabla g_z}{|\mathbf{T}_m|\,|\nabla g_z|}\right). \tag{9}$$

Figure 1 illustrates the vector fields involved in equations (4–9).

Equations (8) and (9) are the basis of the proposed technique since they determine the parameters $|r|$ and α at each station of a profile where both gravity and magnetic data are available. Since both MDR and MI parameters are determined, the proposed method is hereafter referred to as the MDR-MI method, for short.

In summary, except for distortions from noise, the MDR-MI estimates are true over regions along a profile where the Poisson conditions are satisfied. Over such domains, constant values for $|r|$ and α are determined for stations directly above the causative sources as well as in their vicinity. The same estimates are obtained from fields at a different level from the measured one since equations (8) and (9) apply to any position away from the sources. True estimates are obtained either for large isolated sources or complex multisource terranes bearing several inhomogeneities of varied shape and size. Because of such characteristics, the proposed method can be regarded as a robust mapper of the MDR and MI parameters since it can be applied regardless of depth, shape, and number of causative sources. For clarity, to obtain fair estimates the following assumptions must be considered: (1) the sources are homogeneous and elongated (two-dimensional), and (2) all Poisson conditions are satisfied within the sources.

The model in Figure 2 helps us assess the utility of the MDR-MI method in characterizing a multiple-source region whose related anomalies, resulting from the effect of superposition, appear to be very complex (Figure 2c). Despite the complexity of the corresponding anomalies, true MDR and MI values are determined accurately from equations (8) and (9) (Figure 2a). As expected, constant values for both properties are determined in all stations of the profile, either above the sources or in their vicinity. As illustrated in Figure 2b, the intensities $|\mathbf{T}_m|$ and $|\nabla g_z|$ are perfectly correlated when the Poisson conditions are satisfied. This characteristic can be used to identify a region well suited to investigation with the proposed method.

To evaluate the profiles in Figure 2a, the values for $|r|$ and α are numerically computed from the analytic evaluation of both gravity derivatives ($\partial g_z/\partial x$ and $\partial g_z/\partial z$) and magnetic-field components ($T_m^x \equiv \mathbf{e}_x \cdot \mathbf{T}_m$ and $T_m^z \equiv \mathbf{e}_z \cdot \mathbf{T}_m$). Since 2D prisms

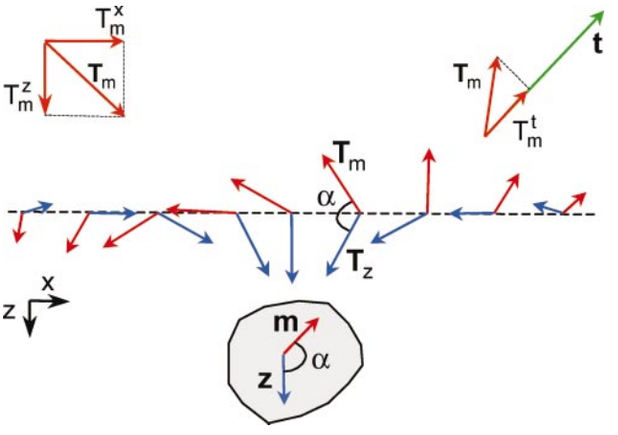

Figure 1. Schematic of the vector fields in equations (4)–(9): $\mathbf{T}_m$ (red) is the vector magnetic field from a source with magnetization along the unit vector **m**; $\mathbf{T}_z$ (blue) is the magnetic field from the same source except by considering a vertical magnetization, **z**. As equation (6) states, the magnitudes of $\mathbf{T}_m$ and $\mathbf{T}_z$ are identical, for any direction **m** and position along a profile. From equations (4) and (9), the angle α of the magnetization is equal to the angle between $\mathbf{T}_m$ and $\mathbf{T}_z$ at any station of a profile. For an inducing field (green) along unit vector **t**, the usually measured total-field anomaly is the component T_m^t. For the sake of graphical representation, the magnitude of $\mathbf{T}_m$ is oversized with respect to the magnitude of the inducing field.

are used, the related analytical solutions are obtained by deriving the corresponding Newtonian gravity potential (Telford et al., 1990). Because of their simplicity and for brevity, these analytical solutions are not included in this paper. After evaluating the gravity derivatives and magnetic components, the magnitude of the fields ∇g_z and $\mathbf{T}_m$ were evaluated according to equations (A-9) and (A-10) of Appendix A.

SYNTHETIC MDR-MI PROFILES

As discussed, the theory behind the MDR-MI method suggests good results when the causative sources are elongated and satisfy the Poisson conditions. However, nothing was said about the method performance where these conditions are violated. Addressing such a matter is not a trivial task since the Poisson conditions can be violated in quite different manners, each representing a particular geological attribute whose characterization could be of interest. To gain insight into the expected MDR-MI performance in more complex environments violating the Poisson conditions, four cases of synthetic MDR-MI responses are presented (Figure 3). These responses were evaluated from a geophysical model consisting of two sets of sources, each side using several 2D prisms. The properties of the prisms on the left side (light gray) are fixed, but the properties of those on the right side (dark gray) are variable. Geologically,

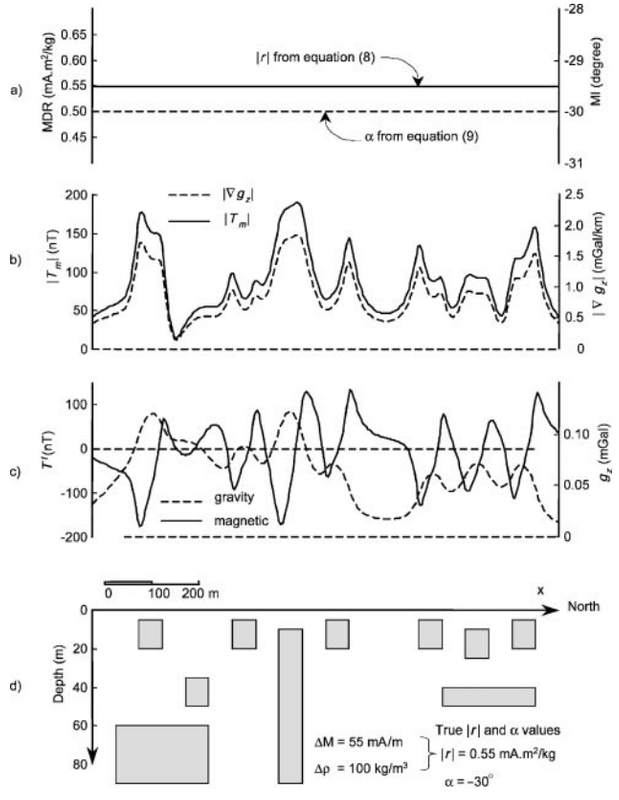

Figure 2. MDR-MI profiles over a multisource prism model obeying the Poisson conditions: (a) MDR (solid) and MI (dashed) values; (b) magnitudes of the vector magnetic field (solid) and gradient of the gravity anomaly (dotted); (c) magnetic (solid) and gravity (dotted) anomalies; (d) cross-section of the 2D prisms and physical property values.

the cases in Figure 3 simulate responses from different types of geological transitions in which the sources in the northern part (right) have different density and magnetic properties relative to the southern part. Southern prisms are magnetized by induction only (inducing field inclination of -30°), and their properties are defined by the following parameters: magnetization inclination, α_1, of -30°; magnetization contrast, $|\Delta\mathbf{M}_1|$, of 55 mA/m; and density contrast, $\Delta\rho_1$, of 100 kg/m^3. Their corresponding MDR value r_1 is then 0.55 mA $\cdot$ m^2/kg.

Similarly, the prisms on the right side (darker ones) are characterized by the parameters α_2, $\Delta\mathbf{M}_2$, and $\Delta\rho_2$. In case 1, the magnetization intensity is $2\,|\Delta\mathbf{M}_1|$, but the MI and density contrast are uniform since $\alpha_2 = \alpha_1$ and $\Delta\rho_2 = \Delta\rho_1$. Because the magnetization contrast is doubled, the MDR parameter for the prisms on the right side, r_2, is 1.10 mA $\cdot$ m^2/kg. In case 2, both magnetization and density contrast are constant, but the magnetization inclination is -90° instead of -30°. The northern source set is thus composed of inhomogeneities with stronger remanent magnetization since their total magnetization inclination differs significantly from the inducing-field inclination. In case 3, both previous conditions are met: the magnetization contrast is doubled, and a remanent magnetization exists. In case 4, only a density variation occurs: the northern prisms exhibit a negative density contrast, but the magnetization parameters are constant.

As Figure 3 shows, at stations far from the transition zone the MDR and MI parameters are correctly determined in all of the tested cases. The rather flat trends over the homogeneous blocks identify the regions satisfying the Poisson conditions. Spurious MDR-MI values only occur close to the transition of source types because in this region the gravity and magnetic fields are mostly affected by the two sets of differing sources. Close to the transition, MDR-MI estimates are only apparent and, as such, may present no direct correspondence with the true properties of the underlying sources. Apparent MDR-MI estimates can even reach values outside the range of the two sets. Nevertheless, the oscillation of the apparent values near the transition zone denotes its presence, which is not very evident in the gravity and magnetic profiles (Figure 3d). It suggests a further application for the proposed method. Besides a physical property profiler, the MDR-MI method might, in some cases, detect the variation between (or within) geological units with MDR or MI contrast.

Another feature observed in Figures 3a and 3b is the rather uncoupled variations exhibited by the MI and MDR profiles. In case 1, for example, the MDR apparent values adequately identify the existing variation, while the MI values only oscillate around the true inclination value. The MI estimates are not severely distorted by the MDR variation, thus establishing the uncoupled characteristic previously described. Uncoupled response is also noted in case 2. In case 3, it allows us to map the joint variation of MDR and MI properties as when isolated variations were considered (cases 1 and 2). In favorable conditions, this MDR-MI uncoupled response could be used to identify which Poisson condition is (are) violated.

Only in case 4 are the MDR-MI apparent values not clearly correlated with the true physical properties of the subjacent prisms. In the MDR profile, the contact position is not clear and peaks occur away from the true position; the MI estimate is around $+30^\circ$ instead of -30°. It occurs because, as shown in equation (9), the substitution of $\nabla\mathbf{g}_z$ by $-\nabla\mathbf{g}_z$, corresponding

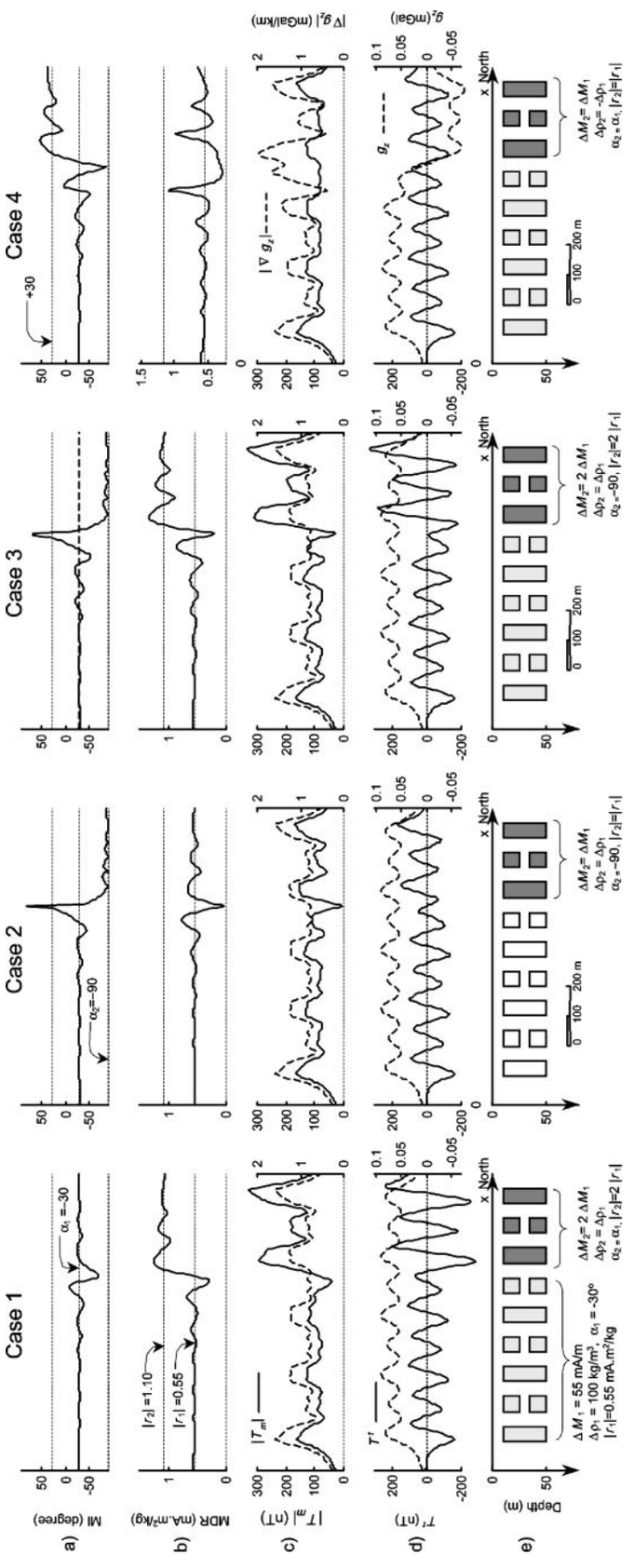

Figure 3. MDR-MI profiles above multisource media representing different types of transition zones (cases 1–4): (a) MI; (b) MDR; (c) vector field magnitudes $|T_m|$ (solid) and $|\nabla g_z|$ (dashed); (d) gravity (dashed) and magnetic (solid) anomalies; (e) prismatic bodies and properties.

to the replacement of $\Delta\rho$ by $-\Delta\rho$, leads to estimates equal to $-\alpha$ because the arcsine is an odd function. To avoid such distortions in MDR-MI applications, the gravity profile must encompass anomalies with only one sign, which can be obtained, for example, by filtering data. Moreover, when the anomalies are negative (negative density contrast), the MI results must be multiplied by -1.

Over homogeneous domains, a higher degree of correlation is observed in the $|\mathbf{T}_m|$ and $|\nabla g_z|$ profiles (Figure 3c). In interpreting real data sets, this criterion can be useful in selecting a profile whose causative sources fulfill the requirements of the MDR-MI method.

DATA PROCESSING CONSIDERATIONS

To be evaluated from equations (8) and (9), the MDR and MI parameters require knowledge of ∇g_z and $\mathbf{T}_m$, which in turn require the gravity anomaly derivatives $\partial g_z/\partial x$ and $\partial g_z/\partial z$ and magnetic field components T_m^x and T_m^z. Unfortunately, routine gravity and magnetic surveys only measure single-field components: the gravity vertical component g_z and the magnetic total-field component $T_m^t \equiv t \cdot \mathbf{T}_m$ or its gradient. The unit vector $\mathbf{t}$ denotes the direction of the geomagnetic field, thus implicitly assuming the use of either a proton-precession or optical-pumping magnetometer, as is usual in modern exploration. Since homogeneous 2D sources are considered, the magnetic field $\mathbf{T}_m$ has components only along the x- and z-axes because the corresponding magnetic potential is invariant along the source strike (y-axis). Therefore, only the $\mathbf{t}$ projection onto the x–z plane is considered when the total-field component is computed. The projected vector $\mathbf{t}_{xz}$, obtained by projecting vector $\mathbf{t}$ onto the x–z-plane, is given by $\mathbf{t}_{xz} = L\mathbf{e}_x + N\mathbf{e}_z$, where $L = \cos(\eta)$, $N = \sin(\eta)$, and $\eta = a\tan\lfloor\tan(I_g)/\cos(D)\rfloor$ is the apparent inclination. The angle I_g is the geomagnetic field inclination, and angle D is such that $D \equiv D_g + S$, where D_g is the geomagnetic declination and S is the source strike, positive clockwise, measured with respect to the north. The profile direction is assumed normal to the source strike.

Because of the intrinsic properties of the potential fields, the required components $\partial g_z/\partial x$, $\partial g_z/\partial z$, T_m^x, and T_m^z can be determined at any point away from the causative sources by applying a suitable set of linear transformations upon the measured anomalies. Further information on the theoretical and practical aspects related to linear transformations of potential fields are provided by Gunn (1975) and Blakely (1995). In the wavenumber domain, the linear transformations can be carried out according to the flowchart presented in Figure 4.

As indicated in Figure 4, the processing routine incorporates a step in which both gravity and magnetic data are upward continued. This operation is included to prevent excessive noise amplification when the gravity gradient magnitude is computed because, in this operation, noise in data is twice amplified: first when the gravity derivatives are evaluated and then when the derivatives are added in equation (A-9). Although generic low-pass filters can be used to control noise amplification, the upward-continuation filter adopted here presents some advantages. The most important one follows the MI and MDR invariance with respect to the level where the gravity and magnetic fields are measured. Continuation to higher levels, however, must be avoided because in regions where the Poisson conditions are violated, the apparent MDR and MI values vary with the vertical distance from the sources (Figure 5). For higher levels, such disturbances are broader and are no longer localized over the contact. Tests conducted using the anomalies of Figure 3 suggest acceptable levels of continuation of up to five or six station spacings above the measuring surface.

Figure 6 shows the MDR and MI estimates obtained in testing the processing routine of Figure 4. In this test, synthetic gravity and magnetic data obtained from case 3 of the model in Figure 3 are used as input. These data are corrupted with additive, uniformly distributed random noise with an amplitude of 1% of the peak-to-peak value of the related anomaly. The anomalies were upward continued by one station spacing

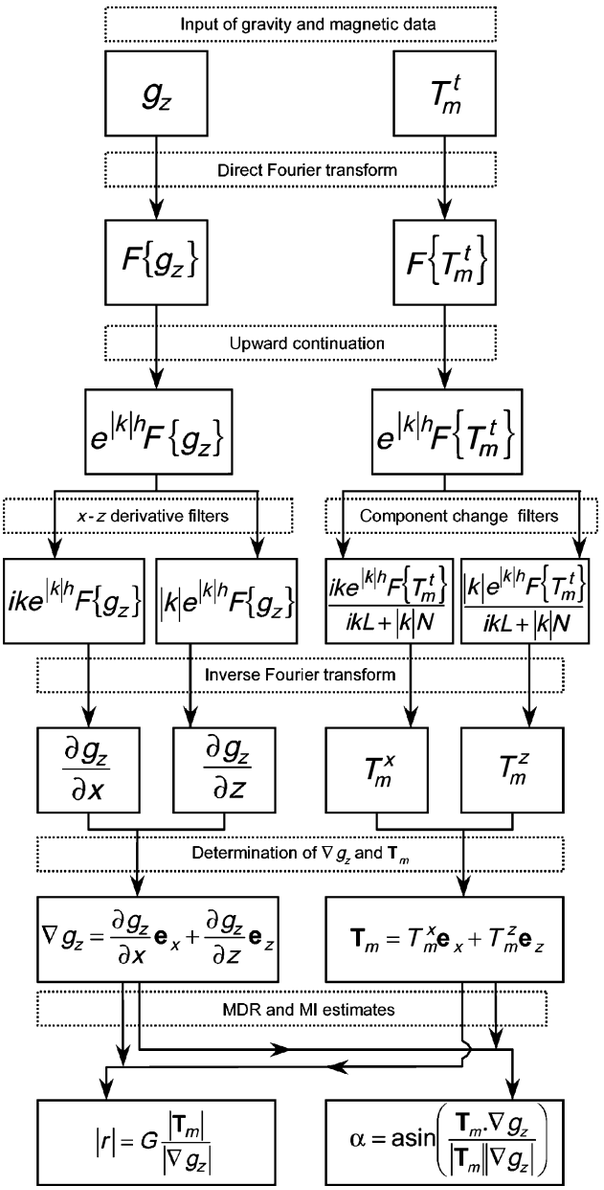

Figure 4. Data processing flowchart to determine MDR and MI parameters. Dotted-line boxes assign instructions, and solid-line ones are the results from such instructions. Further information about the upward continuation and component change filters is found in Gunn (1975) and Blakely (1995).

(3.92 m) above the measuring level (ground surface). As the results in Figure 6 show, the effects of noise are still present in the MDR and MI estimates (squares), but the resulting profiles practically recover the trends defined by the true values (solid line) evaluated directly from the model.

A specialized procedure must be applied when the gravity gradient vanishes. When it happens and a magnetic anomaly exists, the Poisson conditions are not satisfied since the sources of both fields are not common. The MDR is thus undefined, and attempts to estimate it lead to severe numerical instabilities. This problem, however, can be avoided by evaluating equations (8) and (9) only at stations whose $|\nabla g_z|$ values are greater than a prespecified threshold (to be defined by the interpreter).

REAL DATA APPLICATION

My technique was used to interpret two profiles from the eastern portion of the State of Georgia, across the folded Appalachians of North America. These profiles were extracted from the gravity and magnetic data sets compiled by Daniels (2001) and available from the USGS Web site. The compilation of the Bouguer gravity used more than 31 000 stations from Dater et al. (1999) and produced a 3 km gridded data set. The magnetic grid was prepared as part of the USGS effort to create a national airborne magnetic data database. To conform to the national standard of survey elevation, the magnetic data were upward continued to 305 m above ground. After the integration, the magnetic data were interpolated into a 500-m grid corresponding to one-third of the average flight line spacing.

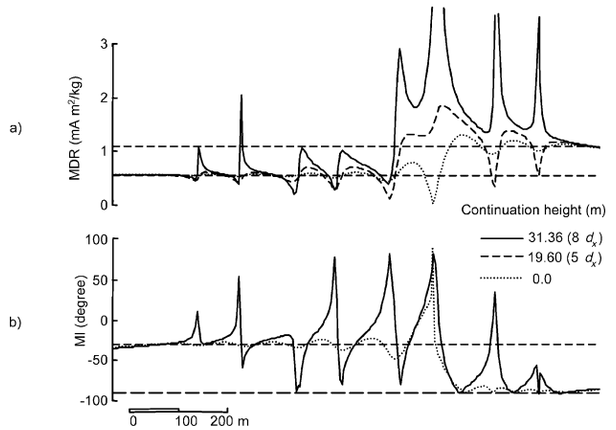

Figure 5. Disturbances in the MDR-MI profiles for different levels above the ground surface: (a) MDR values; (b) MI values. Height levels either expressed in meters and in terms of the station spacing d_x (equal to 3.92 m in this case). For a better visualization, the MI curve for 19.60 m is suppressed in (b). All curves evaluated from the case 3 model, Figure 3.

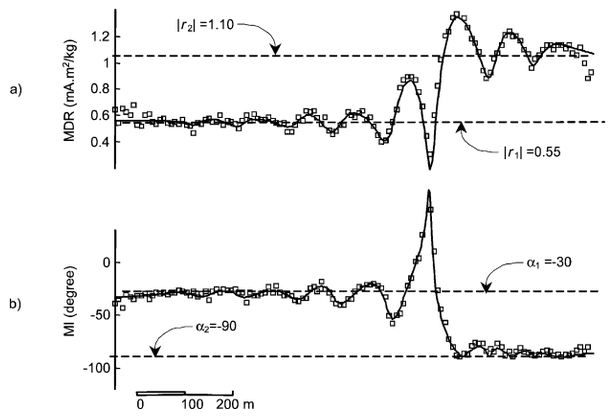

Figure 6. MDR and MI estimates (squares) obtained from the application of the processing scheme of Figure 4 and the corresponding true values (solid line) evaluated from case 3 model, Figure 3: (a) MDR; (b) MI.

General geological and geophysical information for Georgia are provided by Long and Dainty (1985). The Paleozoic Appalachian trend controls the pattern for the gravity and magnetic anomalies in the northeastern portion of the state. In the folded Appalachians and the Blue Ridge province, the regional Bouguer anomaly (Figure 7b) is strong negative, with amplitudes of -40 to -90 mGal. In the Inner Piedmont, a large regional gradient marks the transition from the northwest negative values until the near-zero values at the Charlotte and Carolina slate belts. Over these belts, positive anomalies (15–20 mGal) are associated with shallow mafic rocks. The Brevard thrust fault zone has little gravity expression but is noted in the magnetic anomaly map (Figure 7c). This suggests a no-density contrast for the Brevard (BRV) fault; the contrary is inferred for the Towaliga (TOW) fault. Much lateral transport via thrusting confuses the correlation of the surface geology with deeper structures. The distances related to thrust–transport are at least 200 km for features such as the Blue Ridge and Piedmont sheets (Keller and Hatcher, 1999). The gravity and magnetic anomalies in the Charlotte and Carolina slate belts are more closely correlated with the surface geology.

Figures 8 and 9 show the anomalies and the MDR and MI values along profiles AA′ and BB′. To conform to the specifications of the magnetic data, the gravity values were first upward continued to 305 m and interpolated into a regular spacing of 500 m. To attenuate fields, the gravity and magnetic anomalies were upward continued to 2000 m above the ground. According to the IGRF2000 model, the geomagnetic field inclination is 63° and its declination is $-4°$.

Profile AA′ starts in the southern Inner Piedmont, crosses the Blue Ridge, and enters the folded Appalachians. As shown in Figure 8a, the gravity anomaly presents contributions from both deeper negative-density-contrast sources and shallower positive-density-contrast ones. When computing the gravity gradient, the fields from deeper sources are much attenuated, thus proportionally enhancing the fields from shallow sources. In practical terms, it appears to preclude the application of a regional-residual separation procedure to isolate the anomaly from deeper sources. Over the Blue Ridge, the magnitude of the gravity gradient diminishes and the magnetic magnitude (Figure 8b) increases in relation to the Inner Piedmont. Such combined variation appears in the MDR profile (Figure 8c) as extensive (up to 40 km) flat trends, which, as such, indicates the existence of regions satisfying the Poisson conditions. In the Inner Piedmont the MDR smoothly increases northward, and a rather developed flat line occurs around 0.9 mA.m^2/kg. In the northwestern Blue Ridge a 30-km-long flat trend with values around 2.1 mA $\cdot$ m^2/kg occurs. No expressive variation is observed across the Brevard fault, although near the Cartersville

fault an MDR variation compatible with the contact model response is found.

The MI values suggest induced magnetization over most of the Inner Piedmont but reversed magnetization in the northwestern Blue Ridge. Negative MI estimates, however, must be analyzed carefully since they can be associated with sources violating the Poisson conditions. Figure 10, for example, shows apparent MI reversions caused by localized inhomogeneities with either negative density contrast or reversed magnetization. As this figure suggests, the overall response from a region may be concealed by disturbances from a single shallow source (geological noise), leading to misinterpretation. In fact, the positive magnetic anomaly over the Blue Ridge suggests the existence of sources with normal magnetization.

Profile BB′ in Figure 9 starts in the northeastern coastal plain, crosses the Charlotte and Carolina slate belts, and ends in the southeastern Inner Piedmont. Flat MDR trends are found over both the coastal plain province and the southern portion of the Charlotte and Carolina slate belts. The MDR profile in the southeastern coastal plain identifies two mean values: 0.9 and 0.4 $mA \cdot m^2/kg$ in its southeastern and northwestern boundaries, respectively. However, such a drop in the apparent MDR values can be caused by the existence of a negative-density-contrast source, since a low in the gravity anomaly occurs at the northern coastal plain boundary. Such lowering in the apparent MDR values may occur because the juxtaposition of sources with different density-contrast signs enhances the gravity gradient and thus spuriously diminishes the MDR estimates. The negative values for the apparent MI estimates can also be related to this source. The southeastern Charlotte and Carolina slate belts show no contrast with the northeastern coastal plain. Since the northeastern Charlotte and Carolina slate belts host magnetic sources with no corresponding density contrast, the Poisson conditions are violated there. Their apparent MDR-MI values are then meaningless. The Towaliga fault coincides with the profile position at which a better correlation between the intensities of the gravity gradient and the magnetic field begins in the southeastern Inner Piedmont. However, a localized dense source appears near B′, and the flat behavior previously found in profile AA′ over the Inner Piedmont is interrupted.

CONCLUSIONS

Despite its sound theoretical base and promising results from synthetic tests, the MDR-MI method revealed two main limitations when applied to the interpretation of real gravity and magnetic data. First, the proposed method requires very elongated anomalies, thus requiring a proper profile positioning from an analysis of the maps of the corresponding gravity and magnetic anomalies. Such profile selection is necessary because the apparent MDR-MI values suffer significant disturbances from 3D structures—especially those with the same order of profile length. Very small or very large sources cause, respectively, localized or minor disturbances to the MDR-MI estimates. Upward continuation can attenuate the effects from shallower sources and hence the disturbances they cause. Second, the profile must encompass sources with the same density contrast sign, which implies either negative or positive gravity anomalies but not both simultaneously. It is necessary because very spurious estimates may be found when the gravity anomaly sources present both positive and negative density contrast. In such a situation, the apparent MDR and MI may present little correspondence with the underlying

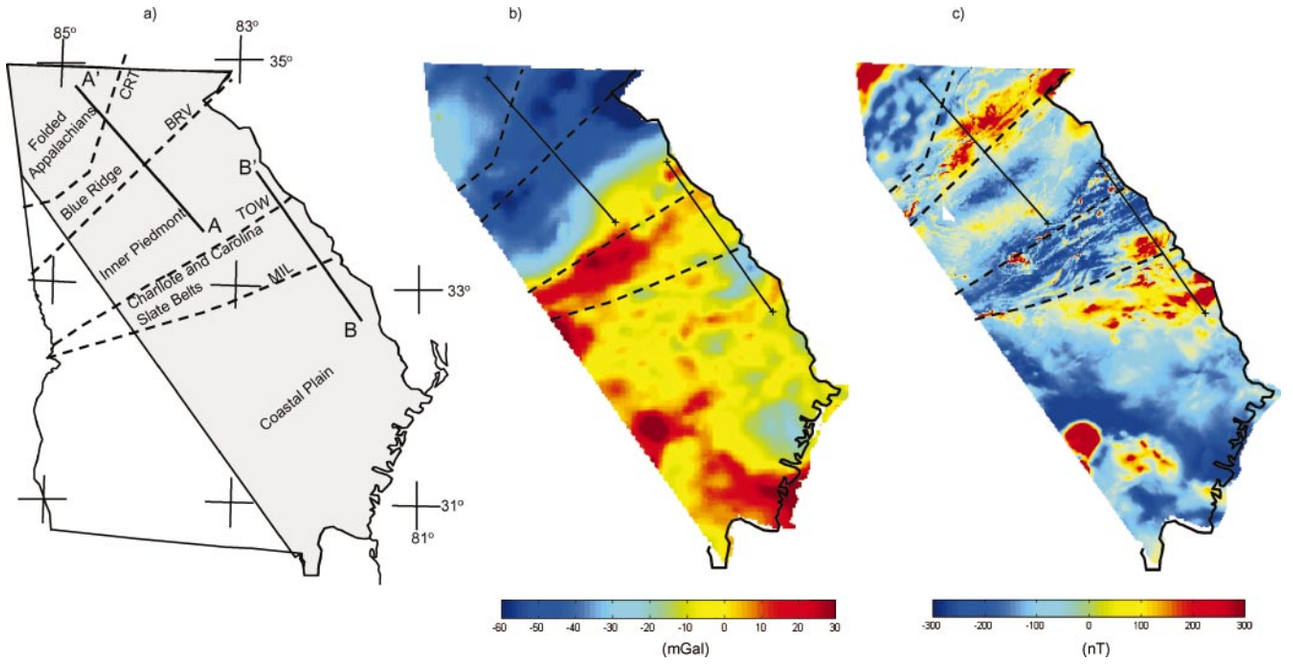

Figure 7. Gravity and magnetic anomaly maps for the eastern portion of Georgia: (a) localization of the profiles and geological framework (after Long and Dainty, 1985): (b) Bouguer gravity anomaly; (c) total-field magnetic anomaly. CRT—Cartersville; BRV—Brevard; TOW—Towaliga; MIL-Middleton-Lowndesville.

sources. Probably, they constitute a significant problem for the proposed method.

Nevertheless, after a proper profile positioning and its length definition, the MDR-MI method can be easily applied and its results promptly interpreted, especially over places where the Poisson conditions are satisfied. Such places are automatically identified from a well-defined flat pattern in both MDR and MI profiles (mainly in the former, as shown in the real data results). Their boundaries can also be inferred since notable variation occurs close to the contacts. Synthetic tests suggest that it may be possible, in some cases, to identify which Poisson condition is being violated, thus furnishing additional information on the rock properties of the subsurface.

Results from the real data application in eastern Georgia suggest the existence of domains satisfying the Poisson conditions across the Appalachian fold belt, a feature practically imperceptible when inspecting the gravity and magnetic anomalies. However, no perfect match between the MDR-MI contacts and the surface geology was found, which may indicate the association of the results with deeper sources situated beneath the Blue Ridge and Inner Piedmont thrust sheets. Two domains

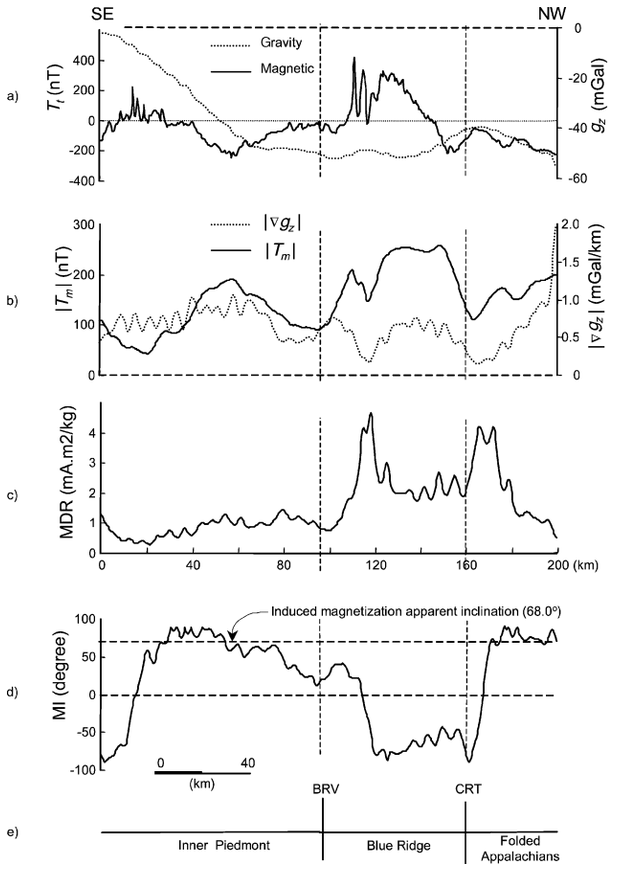

Figure 8. MDR and MI profiles along profile AA′: (a) gravity (dotted) and magnetic (solid) anomalies; (b) field intensities of the gradient of the gravity anomaly (dotted) and magnetic field (solid); (c) apparent MDR; (d) apparent MI; (e) major geological provinces and contacts extracted from Figure 7. CRT and BRV label the Cartersville and Brevard fault zones.

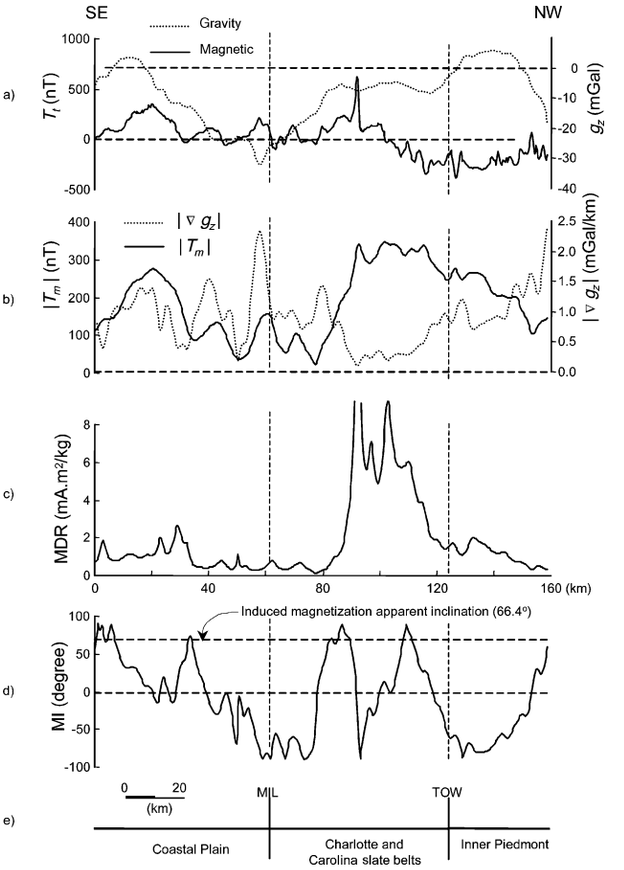

Figure 9. MDR and MI profiles along profile BB′: (a) gravity (dotted) and magnetic (solid) anomalies; (b) field intensities of the gradient of the gravity anomaly (dotted) and magnetic field (solid); (c) apparent MDR; (d) apparent MI; (e) major geological structures. MIL and TOW label Middleton-Lowndesville and Towaliga fault zones.

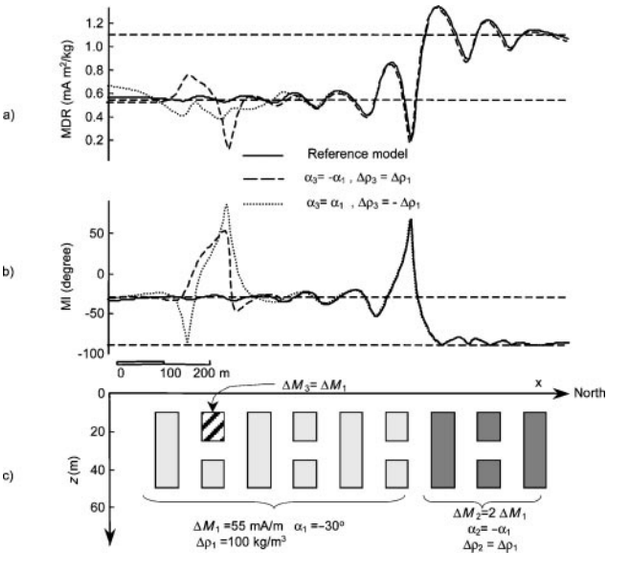

Figure 10. Disturbances on the MDR and MI synthetic estimates caused by a shallower source (dashed prism): (a) MDR; (b) MI; (c) reference model.

with distinct rock property values are detected in the coastal plain province.

ACKNOWLEDGMENTS

Reviews from Afif Saad (Associate Editor), Val Chandler, and two anonymous reviewers much improved the clarity of this paper; the author is grateful to them. This research was supported by grants 301439/91-5 and GTM-01/97-02/01 from CNPq-Brazil.

APPENDIX A

DERIVATION OF EQUATIONS (6) AND (9)

The directional derivative operator $\partial/\partial m$ of equation (1) is defined by

$$\frac{\partial}{\partial m} \equiv \mathbf{m} \cdot \nabla \equiv l\frac{\partial}{\partial x} + k\frac{\partial}{\partial y} + n\frac{\partial}{\partial z}, \tag{A-1}$$

where $\mathbf{m}$ is the unit vector along the magnetization vector; $\nabla \equiv \partial/\partial x\mathbf{e}_x + \partial/\partial y\mathbf{e}_y + \partial/\partial z\mathbf{e}_z$ is the gradient operator in Cartesian coordinates; and (l, k, n) are the direction cosines of $\mathbf{m}$ such that $l = \cos(i_m)\cos(d)$, $k = \cos(i_m)\sin(d)$, and $n = \sin(i_m)$, where i_m is the magnetization inclination and $d = d_m + S$ and additionally where d_m is the magnetization declination and S is the source strike. As used here, the unit vector $\mathbf{e}_y$ lies along the source strike.

For 2D homogeneous sources, only the magnetization component projected onto the x–z-plane effectively contributes to the generation of the magnetic anomaly. This property is determined from the surface integral formulation for the magnetic potential (Blakely, 1995), in which null integrating terms are provided by the tangential component of the magnetization with respect to the body surface. For 2D sources, this property allows us to rewrite the derivative operator in equation (A-1) considering only the magnetization projection onto the x–z-plane. In this case, we can express $\partial/\partial m$ as

$$\frac{\partial}{\partial m} = l'\frac{\partial}{\partial x} + n'\frac{\partial}{\partial z}, \tag{A-2}$$

where $l' = \cos(\alpha)$ and $n' = \sin(\alpha)$ for $\alpha = \text{atan}\,[\tan(i_m)/\cos(d)]$. Angle α is the apparent (or effective) inclination of the magnetization.

By applying the 2D gradient operator in equation (A-2) on the gravity potential in equation (1), the magnetic field $\mathbf{T}_m$ in equation (3) is such that

$$\frac{\mathbf{T}_m}{p} = \left(l'\frac{\partial^2 U}{\partial x^2} + n'\frac{\partial^2 U}{\partial x\partial z}\right)\mathbf{e}_x + \left(l'\frac{\partial^2 U}{\partial x\partial z} + n'\frac{\partial^2 U}{\partial z^2}\right)\mathbf{e}_z. \tag{A-3}$$

The corresponding field $\mathbf{T}_z$ in equation (4) is

$$\frac{\mathbf{T}_z}{p} = \frac{\partial^2 U}{\partial x\partial z}\mathbf{e}_x + \frac{\partial^2 U}{\partial z^2}\mathbf{e}_z. \tag{A-4}$$

By using equations (A-3) and (A-4), the magnitude of the related fields, respectively $|\mathbf{T}_m|$ and $|\mathbf{T}_z|$, are such that

$$\begin{aligned}\left(\frac{|\mathbf{T}_m|}{p}\right)^2 &= \cos^2(\alpha)\left(\frac{\partial^2 U}{\partial x^2}\right)^2 + \sin^2(\alpha)\left(\frac{\partial^2 U}{\partial x\partial z}\right)^2 \\ &\quad + 2\sin(\alpha)\cos(\alpha)\left(\frac{\partial^2 U}{\partial x^2}\right)\left(\frac{\partial^2 U}{\partial x\partial z}\right) \\ &\quad + \cos^2(\alpha)\left(\frac{\partial^2 U}{\partial x\partial z}\right)^2 + \sin^2(\alpha)\left(\frac{\partial^2 U}{\partial z^2}\right)^2 \\ &\quad + 2\sin(\alpha)\cos(\alpha)\left(\frac{\partial^2 U}{\partial z^2}\right)\left(\frac{\partial^2 U}{\partial x\partial z}\right)\end{aligned} \tag{A-5}$$

and

$$\left(\frac{|\mathbf{T}|_z}{p}\right)^2 = \left(\frac{\partial^2 U}{\partial x\partial z}\right)^2 + \left(\frac{\partial^2 U}{\partial z^2}\right)^2. \tag{A-6}$$

Since the gravity potential U obeys the Laplace equation outside the sources, we have for 2D sources $\partial^2 U/\partial x^2 = -\partial^2 U/\partial z^2$ which, when substituted in equation (A-5) and compared with equation (A-6), gives $|\mathbf{T}_z| = |\mathbf{T}_m|$, thus proving equation (6).

To prove equation (9), let us define the angle β as the acute angle between vectors $\mathbf{T}_m$ and $\mathbf{T}_z$, which is given by

$$\cos(\beta) = \frac{\mathbf{T}_m \cdot \mathbf{T}_z}{|\mathbf{T}_m||\mathbf{T}_z|}. \tag{A-7}$$

By considering equations (A-3) and (A-4) and again that U is a harmonic function, we obtain $\cos(\beta) = \sin(\alpha)$. By using equation (4), we obtain

$$\alpha = \text{asin}\left(\frac{\mathbf{T}_m \cdot \nabla g_z}{|\mathbf{T}_m||\nabla g_z|}\right), \tag{A-8}$$

thus proving equation (9). The magnitude of the fields in equation (A-7) is such that

$$|\nabla g_z| = \sqrt{\left(\frac{\partial g_z}{\partial x}\right)^2 + \left(\frac{\partial g_z}{\partial z}\right)^2} \tag{A-9}$$

and

$$|\mathbf{T}_m| = \sqrt{\left(T_m^x\right)^2 + \left(T_m^z\right)^2}. \tag{A-10}$$

By definition, the dot product in equation (A-8) is

$$\mathbf{T}_m \cdot \nabla g_z = \frac{\partial g_z}{\partial x}T_m^x + \frac{\partial g_z}{\partial z}T_m^z. \tag{A-11}$$

Equations (A-9) and (A-10) also can be regarded as the amplitude of the analytical signal, as defined for 2D anomalies by Nabighian (1972, 1974), of the gravity anomaly and the magnetic potential, respectively.

APPENDIX B

MATLAB 5.0 CODE FOR THE ALGORITHM IN FIGURE 4

This code implements the MDR-MI algorithm for the case in which the number of stations is a power of two. To diminish distortions at the profile borders, a simple zero padding scheme

is used. The four MATLAB functions—zeros, length, *fft* and *ifft*—respectively (1) fill a vector with zeros; (2) evaluate the dimension of a vector; (3) apply the fast Fourier transform to a data vector; and (4) evaluate the inverse Fourier transform.

```
function V = mdrmi (x, z, Gz, Tt, INC, dx, hm, hg)
% input
%    x,z = station coordinates (km)
%     Gz = gravity anomaly (mGal)
%     Tt = magnetic anomaly (nT)
%   INC = effective inclination of the inducing field(degree)
%     dx = station spacing
%    hm = height of the magnetic data continuation (km)
%     hg = height of the gravity data continuation (km)
% output
%   MDR = magnetization-to-density ratio (mA.m2/kg)
%      MI = magnetization inclination (degree)
%----------------------- ------------------------
L=cos(INC*0.0175);
N=sin(INC*0.0175);
n=length(x);
m2=1.5*n;n = 4*n;n2 = n/2;
fnyq=0.5/dx;
df=2*fnyq/(n-1);
f=[-fnyq:df:fnyq]';
k=2*pi*f;
K=abs(k);
fh=exp(K*hm);        % upward continuation
fx=i*k.*fh;          % x-derivative
fz=K.*fh;            % z-derivative
ad=i*L*k+N*K;        % t-integration
fX=fx./ad;           % x-component
fZ=fz./ad;           % z-component
% magnetic data filtering
dw=[zeros(m2,1); Tt; zeros(m2,1)]; % zero padding
D=fft(dw,n);
F=[fX(n2+1:n); fX(1:n2)]; a=real(ifft(F.*D,n)); Tx=a(m2+1:
n-m2);
F=[fZ(n2+1:n);   fZ(1:n2)];a=real(ifft(F.*D,n));Tz=a(m2+1:
n-m2);
% gravity data filtering
dw=[zeros(m2,1); Gz; zeros(m2,1)]; % zero padding
fh=exp(K*hg);        % upward continuation
fx=i*k.*fh;          % x-derivative
fz=K.*fh;            % z-derivative
D=fft(dw,n);
F=[fx(n2+1:n); fx(1:n2)];a=real(ifft(F.*D,n));gx=a(m2+1:n-
m2);
F=[fz(n2+1:n); fz(1:n2)];a=real(ifft(F.*D,n));gz=a(m2+1:n-
m2);
% MDR and MI evaluation
TT=sqrt(Tx.*Tx+Tz.*Tz);
GG=sqrt(gx.*gx+gz.*gz);
MDR=0.0000053*TT./GG;
MI=57.2958*a sin([gx.*Tx+gz.*Tz]./[TT.*GG]);
V=[MDR MI];
```

REFERENCES

Baranov, V., 1957, A new method for interpretation of aeromagnetic maps: Pseudo gravity anomalies: Geophysics, **22**, 359–382.

Blakely, R. J., 1995, Potential theory in gravity and magnetic applications: Cambridge University Press.

Bott, M. H. P., and Ingles, A., 1972, Matrix method for joint interpretation of two-dimensional gravity and magnetic anomalies with application to the Iceland-Faeroe Ridge: Geophysical Journal of the Royal Astrological Society, **30**, 55–67.

Chandler, V. W., and Malek, K. C., 1991, Moving-window Poisson analysis of gravity and magnetic data from the Penokean orogen, east-central Minnesota: Geophysics, **56**, 123–132.

Chandler, V. W., Koski, J. S., Hinze, W. J., and Braille, L. W., 1981, Analysis of multisource gravity and magnetic anomaly data sets by moving-window application of Poisson theorem: Geophysics, **46**, 30–39.

Cordell, L., and Taylor, P. T., 1971, Investigation of magnetization and density of a North American seamount using Poisson's theorem: Geophysics, **36**, 919–937.

Daniels, D. L., 2001, Georgia aeromagnetic and gravity maps and data: A web site for distribution of data: USGS Open-File Report **01-0106**, http://pubs.usgs.gov/openfile/of01-106.

Dater, D., Metzger, D., and Hittleman, A., 1999, Land and marine gravity CD-ROM's: National Oceanic and Atmospheric Administration, National Geophysical Data Center.

Garland, G. D., 1951, Combined analysis of gravity and magnetic anomalies: Geophysics, **16**, 51–62.

Grant, F. S., and West, G. F., 1965, Interpretation theory in applied geophysics: McGraw-Hill Book Company.

Gunn, P. J., 1975, Linear transformations of gravity and magnetic fields: Geophysical Prospecting, **23**, 300–312.

Hildebrand, T. G., 1985, Magnetic terranes in the central United States determined from the interpretation of digital data, in W. J. Hinze, ed., The utility of gravity and anomaly maps: SEG, 248–266.

Kanasewich, E. R., and Argawal, R. G., 1970, Analysis of combined gravity and magnetic fields in wave number domain: Journal of Geophysical Research, **75**, 5702–5712.

Keller, G. R., and Hatcher, Jr., R. D., 1999, Some comparisons of the structure and evolution of the southern Appalachian–Ouachita orogen and portions of the Trans-European Suture Zone region: Tectonophysics, **314**, 43–68.

Long, L. T., and Dainty, A. M., 1985, Studies of gravity anomalies in Georgia and adjacent areas of the southeastern United States, in W. J. Hinze, ed., The utility of gravity and magnetic anomaly maps: SEG, 308–319.

Nabighian, M. N., 1972, The analytic signal of two-dimensional magnetic bodies with polygonal cross section: Its properties and use for automated anomaly interpretation: Geophysics, **37**, 507–517.

———1974, Additional comments on the analytic signal of two-dimensional magnetic bodies with polygonal cross section: Geophysics, **39**, 85–92.

Ross, H. P., and Lavin, P. M., 1966, In situ determination of the remnant magnetic vector of two-dimensional tabular bodies: Geophysics, **31**, 949–962.

Telford, W. M., Geldart, L. P., Sheriff, R. E., and Keys, D. A., 1990, Applied geophysics: Cambridge University Press.